Ionics (2020) 26:5405–5415
https://doi.org/10.1007/s11581-020-03679-2

ORIGINAL PAPER

# Selection of nitrogen source and PVP-assisted sol-gel method synthesis of $LiFe_{0.65}Mn_{0.35}PO_4/C$ as cathode material for lithium ion batteries

Shunpan Qiao[1] · Lingzhi Zhu[2] · Enshan Han[2] · Lina Li[1] · Chenyu Du[1] · Yanzhen He[1] · Xu Yang[1] · Jiabao Liu[1]

Received: 24 December 2019 / Revised: 8 June 2020 / Accepted: 29 June 2020 / Published online: 14 July 2020


## Abstract

$LiFe_{0.65}Mn_{0.35}PO_4/C$ composites with porous structure have been successfully prepared through a facile sol-gel method. After comparison, the non-ionic surfactant polyvinylpyrrolidone (PVP) was selected as the best nitrogen source. The structures, morphologies, and electrochemical performances of the composites were characterized by XRD, XPS, SEM, charge/discharge tests, and electrochemical impedance spectroscopy. The $LiFe_{0.65}Mn_{0.35}PO_4/C$ composite which is decorated with suitable amount of PVP has higher discharge capacity and more stable cycling performance. The results show that in the voltage range of 2.5–4.5 V, the discharge capacities of 148, 149.3, 139.3, and 130 $mAhg^{-1}$ in the amount of 20% PVP could be delivered at 0.1, 0.2, 0.5, and 1 C, respectively. A remarkable rate capability was exhibited with 87.84% capacity retention at 1 C rate. The composites owned an optimum performance with a high rate capacity of 146.8 $mAhg^{-1}$ when it returns to 0.1 C after 40 cycles of discharge at different rates.

**Keywords** Lithium-ion battery · Sol-gel method · $LiFe_{0.65}Mn_{0.35}PO_4/C$ composite · PVP

## Introduction

Development of advanced lithium-ion batteries that guarantee high energy density, long-term stability, and low cost has turned into the most important issue due to their versatile use in various devices, such as portable electronics and electric/hybrid vehicles [1–3]. As for the cathode materials of advanced lithium-ion batteries, olivine-structured $LiFePO_4$ has been extensively studied because of its promising properties, including high theoretical capacity, superior safety, long cycle life, and low cost [4–9]. However, $LiFePO_4$ cathodes possess relatively low redox potential (3.4 V versus $Li^+/Li$), thus exhibiting a low energy density. To solve this problem, utilizing several material-processing methods, including conductive layer coating, such as carbon [10–12] polyamide [13], polydopamine [14] melamine [15], poly (vinyl pyrrolidone) [16], could enhance the electronic conductibility of $LiFePO_4$ and then display better electrochemical performance. Simultaneously, controlling the nanoparticles by surfactants could improve the electronic conductivity and ionic conductivity of the materials [17–22], for instance cation surfactant CTAB [23, 24], anion surfactant SDS [25] and neutral polyvinylpyrrolidone (PVP) [26, 27]. However, cationic or anionic surfactants would produce $Na^+$, $Cl^-$, $Br^-$, or $CH_3COO^-$ ions in the solution, which may partially replace $Li^+$, $Fe^{2+}$, $Mn^{2+}$, or $PO_4^{3-}$ in $LiFe_{1-x}Mn_xPO_4/C$ [16, 28–30]. PVP is a kind of widely used non-ionic surfactants, which generate little ion and are affected less by electrolytes, inorganic salts, acids, alkalis, and pH. The addition of

✉ Enshan Han
eshan@hebut.edu.cn

Shunpan Qiao
2269366910@qq.com

Lina Li
1206929370@qq.com

Chenyu Du
491479520@qq.com

Yanzhen He
yzhe87@163.com

Xu Yang
2923932045@qq.com

Jiabao Liu
1031456503@qq.com

[1] School of Chemical Engineering and Technology, Hebei University of Technology, Tianjin 300130, People's Republic of China

[2] Tianjin, China

PVP, can form a carbon-nitrogen layer as a nitrogen source, which can improve the coating structure of the material, thereby enhancing the conductivity of the electrode and the diffusion of lithium ions. Moreover, metal cation doping [31–38], for example $Mn^{2+}$, possessing ionic radius slightly higher than $Fe^{2+}$ and $Fe^{3+}$, would facilitated a wider channel for lithium-ion diffusion, thereby increasing the mobility of lithium ion. Furthermore, major Jahn-Teller lattice distortions induced by $Mn^{3+}$ resulted in poor cycling stability [39, 40]. In recent years, many efforts have been devoted to research the $LiFe_{1-x}Mn_xPO_4$ solid solution system, compared with some other materials [41–45], because of the combination between the advantages of high electronic conductivity of $LiFePO_4$ and high voltage of $LiMnPO_4$. There are two reasons for the material to be superior: one is the relative high potential of $Mn^{3+}/Mn^{2+}$ couple, and the other is the raised potential plateaus of $Fe^{3+}/Fe^{2+}$ couple because of the changed lattice parameters and M–O (M=Mn or Fe) bond lengths [46]. Therefore, various $LiFe_{1-x}Mn_xPO_4$ ($0 < x < 1$) solid solutions were synthesized, such as $LiFe_{0.6}Mn_{0.4}PO_4$ [47–49], $LiMn_{0.5}Fe_{0.5}PO_4$ [50–56], and $LiFe_{0.4}Mn_{0.6}PO_4$ [57], which exhibited much better electrochemical performances than that of the pristine $LiFePO_4$ and $LiMnPO_4$. Zhou et al. [58] successfully synthesized $LiFe_{0.65}Mn_{0.35}PO_4$ materials, which showed better discharge special capacity of 107.46 $mAhg^{-1}$ at 5 C and capacitance conservation rate about 95.47% after 100 cycles at 1 C. This interaction makes the material exhibit excellent electrochemical performances. The structure of $LiFe_xMn_{1-x}PO_4$ is olivine, which is similar to $LiFePO_4$ (or $LiMnPO_4$).

In this article, $LiFe_{0.65}Mn_{0.35}PO_4/C$ was employed as the research substrate synthesized by using the sol-gel method. Based on the different effects of urea, melamine, and PVP on the morphologies and properties of the prepared materials, the optimal material was selected as the nitrogen source. At the same time, the effects of different contents of the substance on the electrochemical performance of the materials were further explored to market needs.

## Experimental

### Synthetic materials

First, $LiFe_{0.65}Mn_{0.35}PO_4/C$ composites were synthesized by adding urea, melamine, and PVP, which respectively accounted for 10% of the mass of the produced materials by using a sol-gel method. After the optimal nitrogen source is selected, different concentrations are explored by adding this substance to the mass of 10%, 20%, 30%, and 40% of the generated material, respectively. The stoichiometric amount of $Mn(CH_3COO)_2{\cdot}4H_2O$ (A.R.), $NH_4H_2PO_4$ (A.R.), $FeCl_2{\cdot}4H_2O$ (A.R.), $CH_3COOLi{\cdot}2H_2O$ (A.R.), $NH_4H_2PO_4$ (A.R.), and $C_6H_8O_7$ (A.R.) (carbon to product molar mass ratio of 3:10) was sequentially dissolved in 150 mL of deionized water, and the corresponding amount of urea, melamine, and PVP (A.R.) was added to the mixed solution in front. The obtained solution was heated in a 70 °C water bath until a gel was formed. The products were further dried at 80 °C in a vacuum oven. After this, the mixture was calcined in a tube furnace at 350 °C for 5 h under argon atmosphere and then cooled to room temperature. The calcined samples were remilled and dried in the same condition with the first milling. After re-agate grinding, the dried powders were calcined in a tube furnace at 750 °C for 10 h under an argon atmosphere and then cooled to room temperature. For comparison, by ensuring that the previous conditions are consistent, a series of material is synthesized by controlling the amount of different PVP additions.

### Preparation of positive film and battery assembly

The as-prepared pure $LiFe_{0.65}Mn_{0.35}PO_4/C$, or $LiFe_{0.65}Mn_{0.35}PO_4/C$, composite (80 wt%) was mixed with acetylene black (10 wt%) and polyvinylidene fluoride (PVDF) (10 wt%) using N-methyl-2-pyrrolidone (NMP) as dispersant to prepare the working electrode. The formed uniformly dispersed slurry was pasted onto an aluminum foil and dried at 102 °C for 12 h in a vacuum oven. The aluminum foil was pressed into a small disk with a diameter of about 10 mm by pressing the tablet machine, and the positive film was obtained. The CR2032 coin cells were assembled in a glove box filled with pure argon with moisture and oxygen levels controlled less than 1 ppm. And the battery was sealed and allowed to stand for 24 h. One mole per liter of $LiPF_6$ in ethylene carbonate (EC), diethyl carbonate (DEC), and dimethyl carbonate (DMC) (1:1:1, *v*/v) was used as the electrolyte solution.

### Physical characterizations and electrochemical tests

The crystal structures were measured by an X-ray diffraction (XRD) analyzer (D8-Fouse, made in Germany), using Cu Ka radiation ranging from 10 to 80° at a scan rate of 12°/min. The materials were analyzed by using X-ray photoelectron spectroscopy (XPS), and the atomic and nitrogen species of the samples were obtained through this process. The microstructure and particle size distribution were examined by using the scanning electron microscopy (SEM, Nova Nano SEM 450 FEI). The CT-2001 battery test system was used to evaluate the constant current charge/discharge performance of the material, with a voltage range of 2.5–4.5 V (versus $Li^+/Li$). The specific surface areas and the pore size distributions were evaluated by using a Brunauer-Emmett-Teller (BET) test analyzer (ASAP 2460, USA). The C content and N content of the material are tested and analyzed by using an element analyzer (American Thermoelectric Company FLASHEA1112).

The cyclic voltammograms (CV) and electrochemical impedance spectroscopy (EIS) measurements were both carried on a CHI660C electrochemical workstation at room temperature. The CV was tested in the voltage range of 2.5–4.5 V (versus $Li^+/Li$) at a scan rate of 0.1 $mVs^{-1}$, and the EIS measurements were in the frequency range from 0.01 Hz to 100 kHz. The software ZsimpWin 3.10 was used to analyze the EIS data.

## Results and discussion

### Searching of the suitable nitrogen source

#### Structure and morphology

XRD was measured to detect the purity of the samples synthesized by different nitrogen sources. Figure 1 shows the XRD patterns for the investigated lithium iron manganese phosphate samples after adding urea, melamine, and PVP. The XRD peaks of the four samples are basically consistent with the standard peaks of the olivine-type $LiFePO_4$ (JCPDS No. 40−1499). The three kind of the added N sources maintained the crystal structure of the $LiFe_{0.65}Mn_{0.35}PO_4/C$ material. The sharp peaks illustrated the well-developed and perfect $LiFe_{0.65}Mn_{0.35}PO_4/C$ crystallites. The addition of urea, melamine, and PVP exhibited little or no effect on the crystallization of $LiFe_{0.65}Mn_{0.35}PO_4$ within a certain concentration range. The carbon in the composite is amorphous, since no diffraction peaks of crystalline carbon could be detected.

The lattice parameters are listed in Table 1. The similar parameters of the crystal certified that the introduction of urea, melamine, and PVP into the system could not change the crystal structure. Adding the nitrogen source could provide a larger ionic radius space for migration and accelerate the diffusion of lithium ions due to the larger volume. Thus, the utilization of PVP possessing the largest volume into the system was a benefit for the ion transfer.

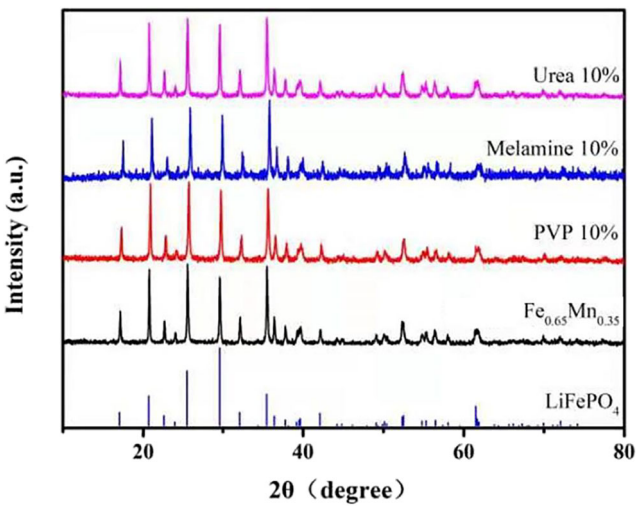


**Fig. 1** XRD patterns of $LiFe_{0.65}Mn_{0.35}PO_4/C$ (adding urea, melamine, and PVP, which respectively accounted for 10% of the mass of the produced materials)

**Table 1** Lattice parameters of the prepared samples

| Samples | a/(Å) | b/(Å) | c/(Å) | V(Å$^3$) |
|---|---|---|---|---|
| $Fe_{0.65}Mn_{0.35}$ | 10.3766 | 6.0422 | 4.7125 | 295.4649 |
| $Urea_{10\%}$ | 10.3781 | 6.0429 | 4.7128 | 295.5610 |
| $Melamine_{10\%}$ | 10.3792 | 6.0440 | 4.7127 | 295.6370 |
| $PVP_{10\%}$ | 10.3807 | 6.0403 | 4.7151 | 295.6532 |

SEM images in Fig. 2 illustrated that the three materials prepared by different N sources exhibited significant difference. The material added with 10% PVP possessed porous structure obviously among particles, which could improve the specific surface area and make it easier for the electrolyte penetrating into the material. However, the other two samples were just slightly lumpy.

#### Physical characterization

The different performances among these three samples are evidenced by the CV curves in Fig. 3a $LiFe_{0.65}Mn_{0.35}PO_4/C$ displayed two pairs of redox peaks which corresponded to the $Fe^{3+}/Fe^{2+}$ and $Mn^{3+}/Mn^{2+}$, respectively. The redox peak symmetry of the two groups of prepared materials with 10% PVP addition was better, which implied that the sample possessed good electrochemical performances. The AC impedance spectra of three different additives for electrodes to further detect the conductivity are shown in Fig. 3b. The charge transfer resistance of the three samples were 535.2 Ω, 881.8 Ω, and 1601.2 Ω. Figure 3c and d depict charge and discharge curves under 0.1 C the first time, and the rate performance of three samples under different rates. The sample with 10% PVP addition exhibited higher discharge capacity and better rate performances than those of other sample. Therefore, PVP was selected as the research object to be further analyzed.

### The effects of different concentrations

#### Structure and morphology

XRD patterns of these samples and standard $LiFePO_4$ are shown in Fig. 4. The positions and relative intensities of the diffraction peaks are close to the pattern of standard $LiFePO_4$ in the bottom. The reflection peaks were sharp and narrow, indicating good crystalline degree of the samples, and there is no diffraction peak of carbon in Fig. 4. The lattice parameters are presented in Table 2. Similarly, the unit cell volume of all samples has increased slightly compared with $Fe_{0.65}Mn_{0.35}$, which not only provided a larger ionic radius for ion migration but also accelerated the extraction and insertion of lithium

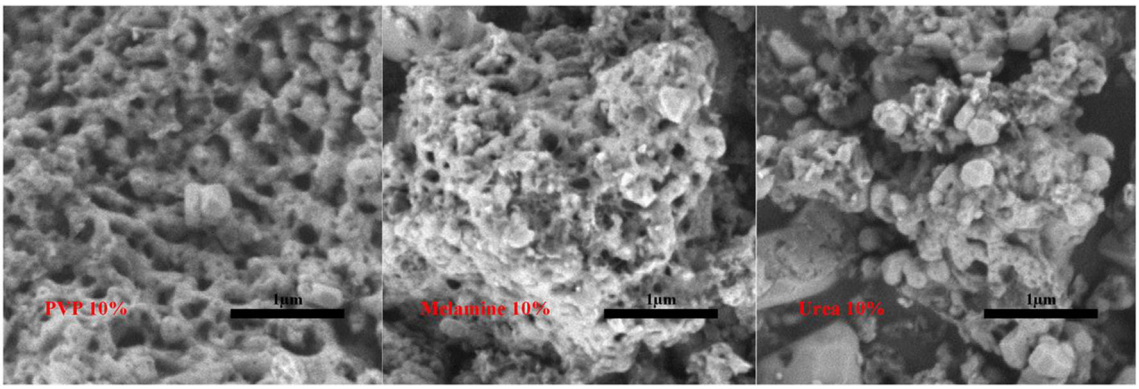


**Fig. 2** SEM images of $LiFe_{0.65}Mn_{0.35}PO_4/C$ (adding urea, melamine, and PVP, which respectively accounted for 10% of the mass of the produced materials)

ions. The 20% volume of the PVP could reach up to the largest volume, and adding more PVP into the system would lead to the decrease of the volume.

The samples with different levels of PVP could exhibit obvious porous structures without blocky structure (Fig. 5). Compared with the standard $Fe_{0.65}Mn_{0.35}$, many pores occurred on the surface of the sample with PVP, which meant that the pyrolysis of PVP in the calcining process would promote the formation of porous structure. It is very likely that the formed nitrogen-doped carbon coating could effectively improve the electronic conductivity and electrochemical performances of $LiFe_{0.65}Mn_{0.35}PO_4/C$.

The XPS spectrum of the sample prepared with PVP content of 20% by mass of the synthetic material is listed in Fig. 6a. The peaks of $Li_{1s}$, P1s, P2s, C1s, N1s, O1s, Fe2p, and Mn2p3 could be clearly seen in Fig. 6a. C1s peaks around 290 eV, and N1s peaks around 400 eV, indicating that the carbon and nitrogen elements indeed presented in the sample.

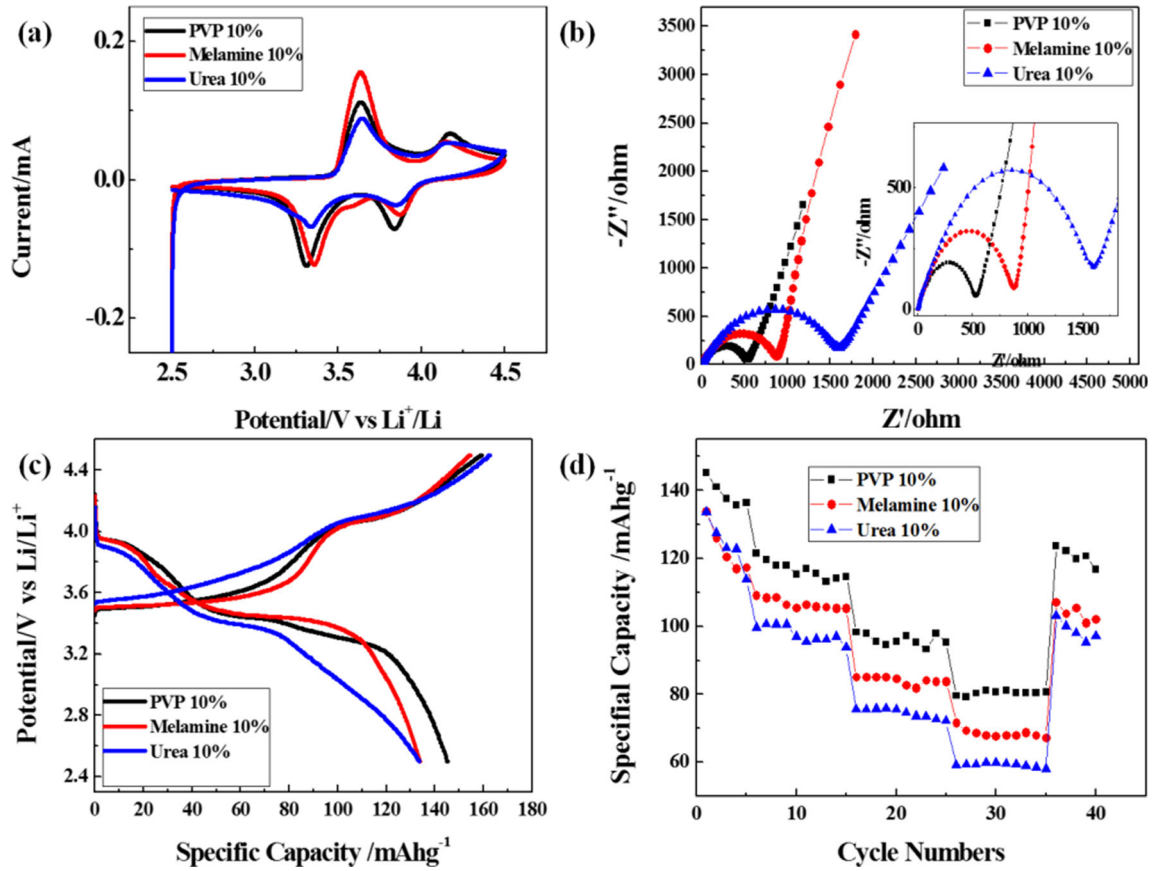


**Fig. 3** Electrochemical performance of the different nitrogen sources. **a** CV curves at a scan rate of 0.1 $mVs^{-1}$. **b** Nyquist plots with testing frequency range from 0.01 Hz to 100 kHz. **c** Initial charge/discharge profiles between 2.5 and 4.5 V under 0.1 C. **d** Rate performance from 0.1 to 1 C

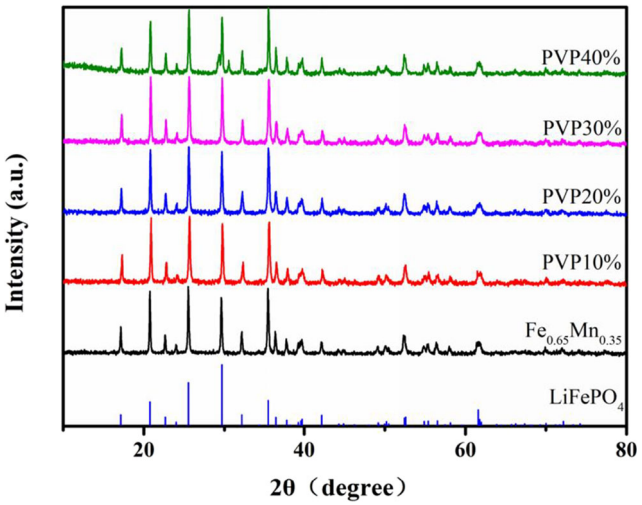


**Fig. 4** XRD patterns of $LiFe_{0.65}Mn_{0.35}PO_4/C$ (pure sample, and 10%, 20%, 30%, and 40% PVP addition)

The high-resolution N1s spectrum (Fig. 6b) displayed three different states of N element: pyridinic N (398.5 eV), pyrrolic N (400.9 eV), and graphitic type of N (401.6 eV) [59], and the peak area ratios were 27.70%, 44.70%, and 27.21%, respectively. Generally, the pyridine-type nitrogen and pyrrole-type nitrogen are considered as defective nitrogen; many vacancies and dangling bonds formed with the N atom doping, which could provide active sites for lithium ions to be embedded. The graphite-type nitrogen could improve the conductivity and electrochemical activity of the material [60].

In order to further investigate the porous structure, $N_2$ adsorption/desorption isotherms are measured. As shown in Fig. 7, the adsorption-desorption isotherms of the samples all show a type IV adsorption-desorption isotherm with a H3-type hysteresis loop at the range of 0.4–1.0 $P/P_0$ [56], indicating the mesoporous structure of the material. Moreover, we can see that the pore size distribution curve is between 2 and 140 nm from the sample BJH pore size distribution curve. Most pore sizes are between 2 and 20 nm; a small part of the pore sizes is between 20 and 50 nm. Simultaneously, the structural property parameters are presented in Table 3.

The specific surface areas of all samples calculated using the method are 15.29 $m^2g^{-1}$, 14.65 $m^2g^{-1}$, 19.88 $m^2g^{-1}$, 11.89 $m^2g^{-1}$, and 14.99 $m^2g^{-1}$, respectively. Compared with other samples, when the amount of PVP added is 20%, it has a larger surface area and pore volume. At the same time, the surface area and pore volume of the sample are 0.13 $cm^3g^{-1}$ and 22.04 nm, respectively, which provide a larger contact area for active materials and electrolytes, and it is more conducive to ion migration and accelerates the extraction and insertion of lithium ions. It could effectively improve the electronic conductivity and electrochemical performances of the material.

**Table 2** Lattice parameters of the prepared samples

| Samples | a/(Å) | b/(Å) | c/(Å) | V(Å$^3$) |
|---|---|---|---|---|
| $Fe_{0.65}Mn_{0.35}$ | 10.3766 | 6.0422 | 4.7125 | 295.4649 |
| $PVP_{10\%}$ | 10.3807 | 6.0403 | 4.7151 | 295.6532 |
| $PVP_{20\%}$ | 10.3795 | 6.0448 | 4.7143 | 295.7859 |
| $PVP_{30\%}$ | 10.3792 | 6.0433 | 4.7145 | 295.7144 |
| $PVP_{40\%}$ | 10.3767 | 6.0433 | 4.7137 | 295.5933 |

The C content and N content of the sample are shown in Table 4. Since the added raw material PVP is a polymer, we can see that with the continuous addition of PVP, the C content is continuously increasing, while the N content is constantly decreasing. The changes in the content of the two elements present a more reasonable change trend. When the amount of PVP is 20%, the N content of the synthetic material is relatively higher, which is beneficial to the synthesis of carbon and nitrogen layer.

## Physical characterizations

For further understanding the electrochemical properties, the CV curves of $LiFe_{0.65}Mn_{0.35}PO_4/C$ (pure sample and different PVP additions) are given in Fig. 8a. The CV curves of both electrodes possessed two redox peaks at ~ 3.5 and ~ 4.1 V versus $Li/Li^+$. When PVP was added at 20% content, two pairs of redox potential peaks appeared at approximately 4.118/3.881 V and 3.614/3.370 V, which accorded with the redox couple of $Mn^{3+}/Mn^{2+}$ and $Fe^{3+}/Fe^{2+}$. Simultaneously, the redox peaks were sharper and more symmetric, indicating the improved reversibility, decreased polarization, and enhanced kinetic process for lithium-ion insertion/extraction, which was consistent with a smooth voltage platform. Figure 8c showed the initial charge and discharge capacity of $LiFe_{0.65}Mn_{0.35}PO_4/C$ (pure sample and different amount of PVP added) at a rate of 0.1 C between 2.5 and 4.5 V. The 20% of PVP into the system could increase charge and discharge capacity than those of the original $LiFe_{0.65}Mn_{0.35}PO_4/C$ at a low rate of 0.1 C, which could reach up to 148.0 $mAhg^{-1}$, and both displayed relatively stable charging and discharging platforms. Comparing the cycle of $LiFe_{0.65}Mn_{0.35}PO_4/C$ (pure sample and different PVP addition) materials charged at 0.1 C rates and discharged at 0.1C, 0.2 C, 0.5 C, and 1.0 C rates performance curve in Fig. 8d, at all charge and discharge rates, only pure samples and PVP with 20% addition possessed better cycle rate performance. Other samples experienced more severe attenuation at high magnifications. The first-cycle discharge capacity of the material $LiFe_{0.65}Mn_{0.35}PO_4/C$ (pure sample and 10%, 20%, 30%, and 40% PVP addition) was approximately 145.3, 145.1, 148.0, 143.5, and 120.5 $mAhg^{-1}$, respectively at 0.1 C. The discharge capacity of the first cycle measured at various rates with the decreasing order pure sample > 20% > 10% > 30% > 40% at 1 C. After returning to 0.1 C, the capacity retention rates are 95.46%, 85.25%, 99.19%, 83.48%, and

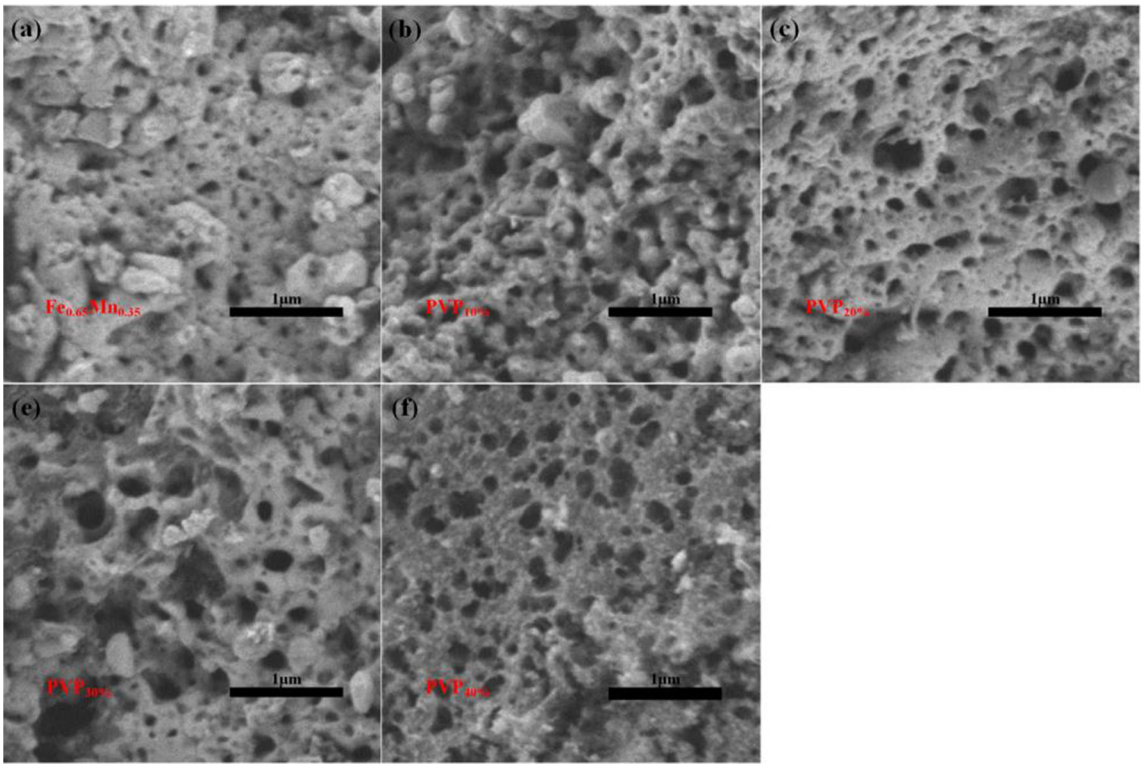


**Fig. 5** SEM images of $LiFe_{0.65}Mn_{0.35}PO_4/C$ (pure sample, and 10%, 20%, 30%, and 40% PVP addition)

76.10%, respectively. By comparison, $LiFe_{0.65}Mn_{0.35}PO_4/C$ (PVP addition amount is 20%) owned better rate performance. Figure 8d showed the AC impedance spectrum of the prepared sample $LiFe_{0.65}Mn_{0.35}PO_4/C$ (pure sample and different PVP addition amount) material. Figure 8b depicts the equivalent circuit Int. Each Nyquist diagram consists of three parts: the abscissa intercept point in the high-frequency region, the semicircular region in the intermediate-frequency region, and the inclined straight line in the low-frequency region. The fitting results of the electrochemical impedance curve data are shown in Table 5. Electrolyte resistance, electrode interface resistance, and charge transfer resistance are represented by $R_s$, $R_{sei}$, and $R_{ct}$, respectively. $R_{ct}$ values of $LiFe_{0.65}Mn_{0.35}PO_4/C$ (pure samples and different PVP addition amounts) were 716.4 Ω, 535.2 Ω, 430.7 Ω, 500.7 Ω, and 843.7 Ω, respectively. When PVP was added at 20%, the smallest charge transfer resistance appeared compared with other samples. The charge transfer resistance of the doped material was smaller than that of the pure-phase material, consistent with the results of previous electrochemical tests. This showed that adding appropriate amount of PVP could effectively reduce the charge transfer resistance.

$$D_{Li+} = R^2 \times T^2 / \left(2A^2 \times n^2 \times F^4 \times C^2 \times \sigma^2\right) \quad (1)$$

Figure 9a presents the linearity of $Z'$ and $\omega^{-1/2}$ of the prepared sample fit of the graph. The lithium-ion diffusion coefficient was calculated by using formula (1), where $R$ is the gas constant (8.314 $Jmol^{-1}$ $K^{-1}$), $T$ is the absolute temperature, $A$ is the surface area of the positive electrode (estimated to be

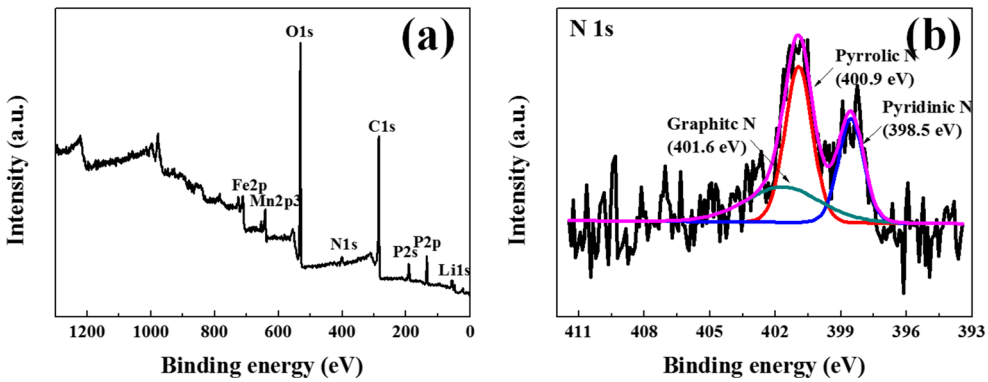


**Fig. 6** XPS spectra of $LiFe_{0.65}Mn_{0.35}PO_4/C$ (adding PVP which accounted for 20% of the mass of the generated material)

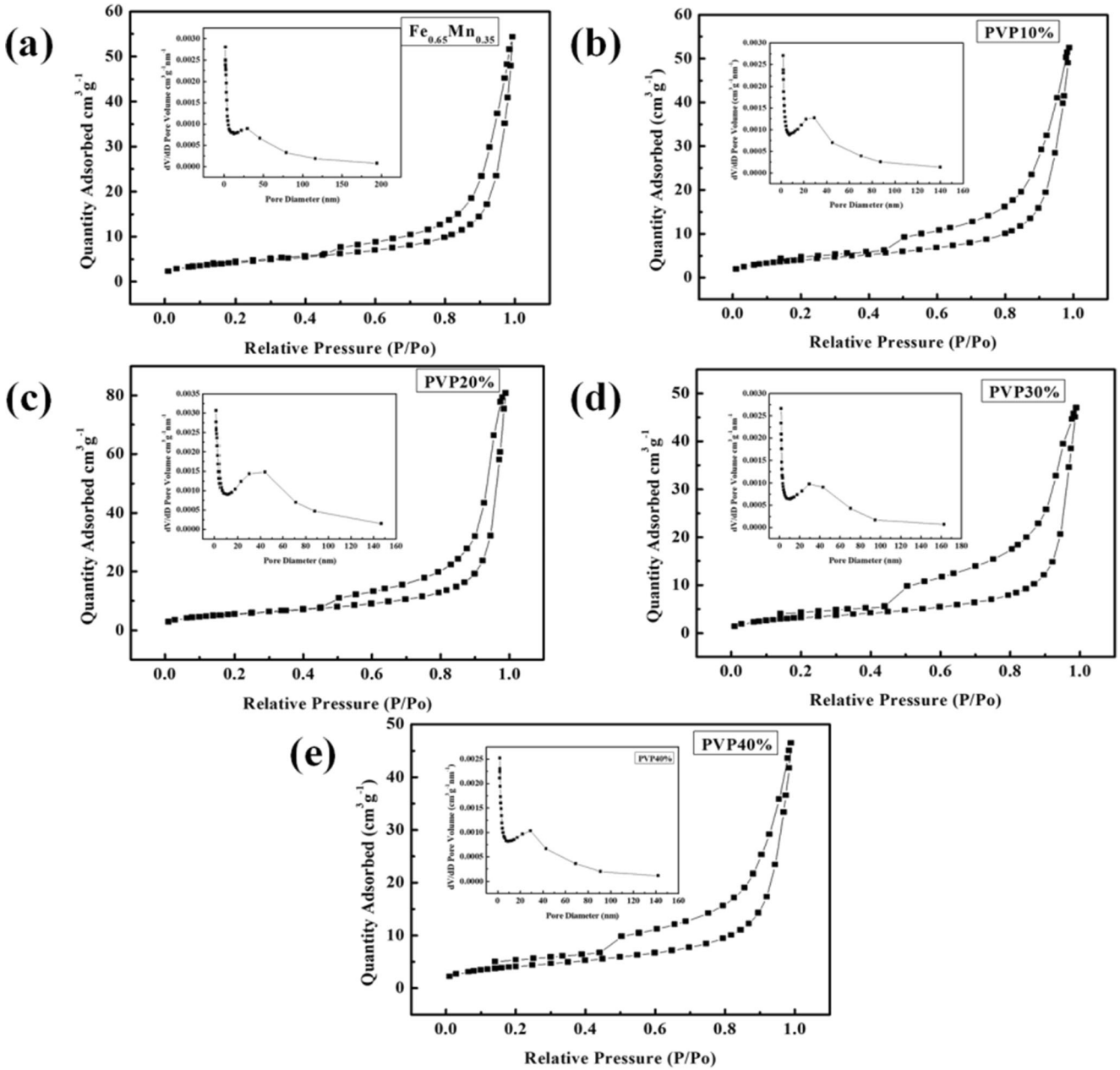


**Fig. 7** $N_2$ adsorption-desorption isotherms and the BJH pore size distribution curves of $LiFe_{0.65}Mn_{0.35}PO_4/C$ (pure sample, and 10%, 20%, 30%, and 40% PVP addition)

**Table 3** Specific surface area, pore volume, and average pore size of prepared samples

| Samples | $S_{BET}$ ($m^2g^{-1}$) | $V_{pores}$ ($cm^3g^{-1}$) | $d_{pores}$ (nm) |
|---|---|---|---|
| $Fe_{0.65}Mn_{0.35}$ | 15.29 | 0.09 | 19.37 |
| $PVP_{10\%}$ | 14.65 | 0.08 | 18.77 |
| $PVP_{20\%}$ | 19.88 | 0.13 | 22.04 |
| $PVP_{30\%}$ | 11.89 | 0.08 | 20.16 |
| $PVP_{40\%}$ | 14.99 | 0.07 | 18.13 |

0.785 $cm^2$), $n$ is the number of electrons required to participate in the unit reaction, $F$ is the Faraday constant (96,485.33 $Cmol^{-1}$), C (0.0288 mol $cm^{-3}$) [58] is the application of lithium ions in $LiFePO_4$, and $\sigma$ is the Wahlberg factor

**Table 4** C and N element contents of the prepared samples

| Samples | C (%) | N (%) |
|---|---|---|
| $PVP_{10\%}$ | 12.88 | 2.71 |
| $PVP_{20\%}$ | 14.10 | 2.15 |
| $PVP_{30\%}$ | 14.57 | 1.76 |
| $PVP_{40\%}$ | 14.91 | 1.44 |

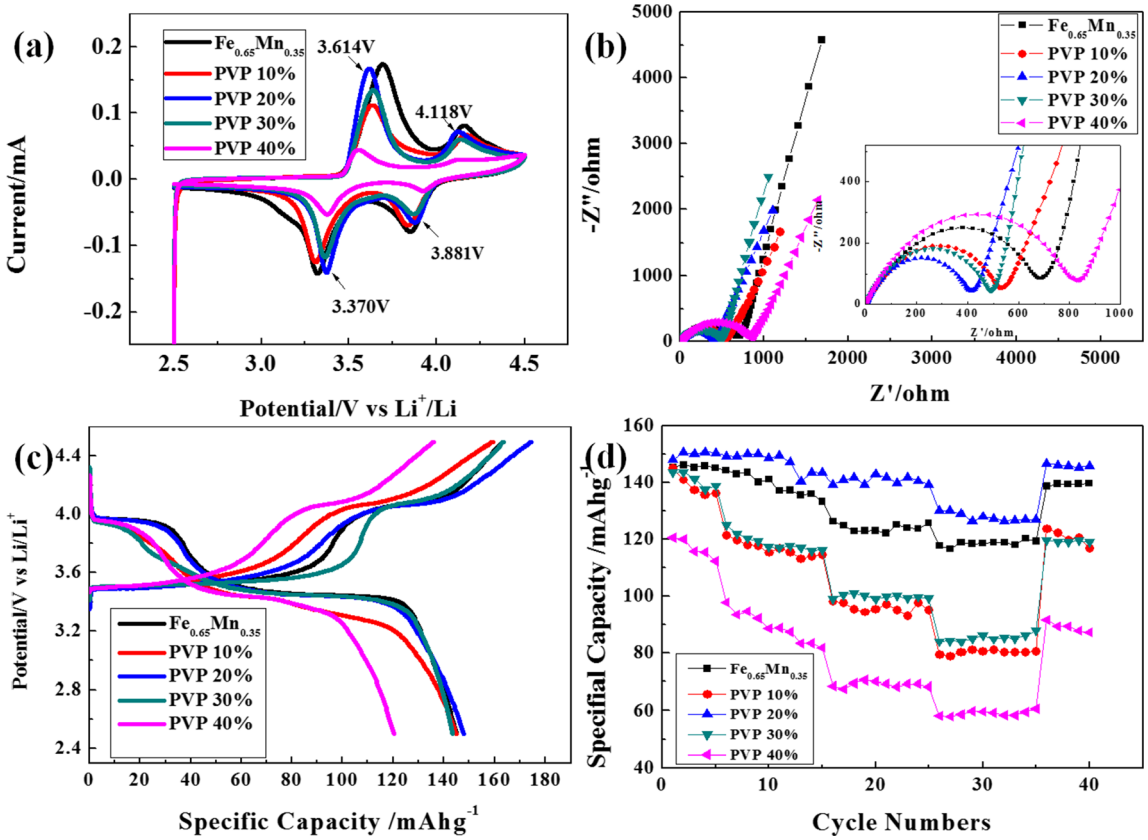


**Fig. 8** Electrochemical performance of the pure sample and different PVP additions. **a** CV curves at a scan rate of 0.1 $mVs^{-1}$. **b** Nyquist plots with testing frequency range from 0.01 Hz to 100 kHz. **c** Initial charge/discharge profiles between 2.5 and 4.5 V under 0.1 C. **d** Rate performance from 0.1 to 1 C

(Fig. 8 slope) [61]. Obviously, the proper addition of PVP could effectively improve the lithium-ion diffusion coefficient. The $Li^+$ diffusion coefficients of each sample were $1.091 \times 10^{-14}$ $cm^2s^{-1}$, $2.972 \times 10^{-14}$ $cm^2s^{-1}$, $2.342 \times 10^{-14}$ $cm^2s^{-1}$, $3.340 \times 10^{-14}$ $cm^2s^{-1}$, and $1.867 \times 10^{-14}$ $cm^2s^{-1}$, respectively. All the PVP-added samples increased the $Li^+$ diffusion coefficient, which was consistent with reports from some articles in previous studies [16].

## Conclusion

In summary, according to a simple sol-gel method, we doped PVP, melamine, and urea with the material mass fraction of 10% to get the final product. PVP was chosen as the nitrogen source to further research by comparison and selection. Comparing with different amounts of materials synthesized by PVP, $LiFe_{0.65}M_{0.35}PO_4/C$ which was synthesized by 20% PVP has the best electrochemical performance. It can effectively reduce the impedance of the material and increase the specific capacity and cycle stability of the material. The first discharge at 0.1 C reached 148.0 $mAhg^{-1}$, and that of 1 C was 130.0 $mAhg^{-1}$. When charged and discharged are at different rates and returned to 0.1 C, the capacity retention rate reached 99.20%. In addition, the $R_{ct}$ values and the $Li^+$ diffusion coefficient of this sample were 430.7 Ω and $2.342 \times 10^{-14}$ $cm^2s^{-1}$, respectively. The excellent electrochemical performance should be attributed to the formation of the carbon-

**Table 5** EIS fitting data of the pure sample and different PVP additions

| Samples | $R_s$ (Ω) | $R_f$ (Ω) | $R_{ct}$ (Ω) | $D_{Li+}$ ($cm^2s^{-1}$) |
|---|---|---|---|---|
| $Fe_{0.65}Mn_{0.35}$ | 2.408 | $5.802 \times 10^{14}$ | 716.4 | $1.091 \times 10^{-14}$ |
| $PVP_{10\%}$ | 2.613 | 554.1 | 535.2 | $2.972 \times 10^{-14}$ |
| $PVP_{20\%}$ | 3.102 | 6565 | 430.7 | $2.342 \times 10^{-14}$ |
| $PVP_{30\%}$ | 3.155 | $2.422 \times 10^{12}$ | 500.7 | $3.340 \times 10^{-14}$ |
| $PVP_{40\%}$ | 2.978 | $1.922 \times 10^{12}$ | 843.7 | $1.867 \times 10^{-14}$ |

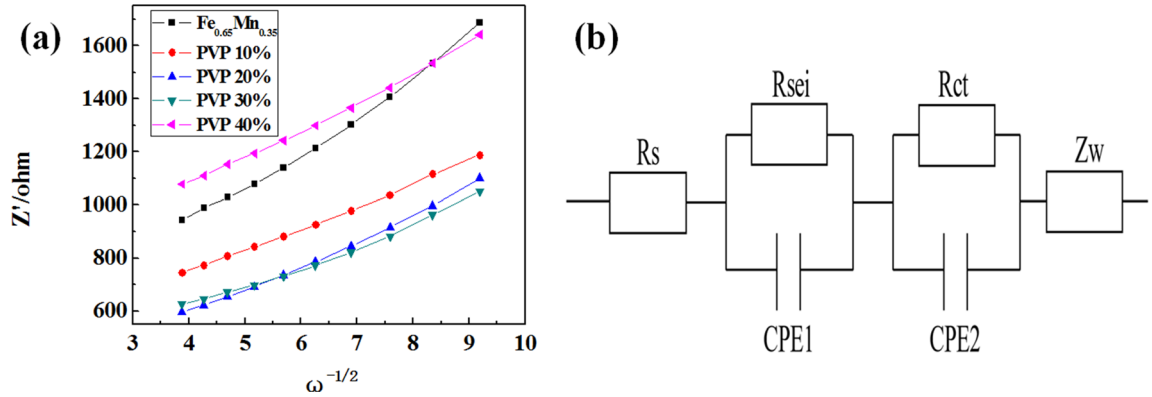


**Fig. 9** Linear fitting of the Z′ versus $\omega^{-1/2}$ relationship (**a**) and equivalent circuit diagram (**b**) of $LiFe_{0.65}Mn_{0.35}PO_4/C$

nitrogen layer as a nitrogen source, thereby enhancing the electrode's electrical conductivity and lithium-ion diffusion. The excellent cycle stability can be attributed to its use as a surfactant, which prevents colloidal particles and carbon sources from agglomerating to form well-crystallized particles.

## References


1. Whittingham MS (2004) Lithium batteries and cathode materials. Chem Rev 35(50):4271–4301
2. Armand M, Tarascon JM (2008) Building better batteries. Nature 451(7179):652–657
3. Xu J, Zhang L, Wang Y, Chen T, Alshroofy M, Cheng Y (2017) Unveiling the critical role of polymeric binders for silicon negative electrodes in lithium-ion full cells. ACS Appl Mater Interfaces 9(4): 3562–3569
4. Padhi AK, Nanjundaswamy KS, Goodenough JB (1997) Phospho-olivines as positive-electrode materials for rechargeable lithium batteries. J Electrochem Soc 144(4):1188–1194
5. Fergus JW (2010) Recent developments in cathode materials for lithium ion batteries. J Power Sources 195(4):939–954
6. Scrosati B, Garche J (2010) Lithium batteries: status, prospects and future. J Power Sources 195(9):2419–2430
7. Li Z, Zhang D, Yang F (2009) Developments of lithium-ion batteries and challenges of $LiFePO_4$ as one promising cathode material. J Mater Sci 44(10):2435–2443
8. Bauer EM, Bellitto C, Righini G, Pasquali M, Dellera A, Prosini PP (2005) A versatile method of preparation of carbon-rich $LiFePO_4$: a promising cathode material for Li-ion batteries. J Power Sources 146(1):544–549
9. Pasquali M, Dellera A, Prosini PP (2009) Fitting of the voltage–$Li^+$ insertion curve of $LiFePO_4$. J Solid State Electrochem 13(12): 1859–1865
10. Kai W, Yang J, Ren W, Feng P (2016) Soft conductive carbon enables depolarization of $LiFePO_4$ cathodes to enhance both capacity and rate performances of lithium ion batteries. J Power Sources 331:232–239
11. Xu Y, Mao J (2015) Improve electrochemical performance of $LiFePO_4/C$ cathode by coating $Ti_2O_3$ through a facile route. Ionics 21:3159–3167
12. Tian X, Zhou Y, Tu X, Zhang Z, Du G (2017) Well-dispersed $LiFePO_4$ nanoparticles anchored on a three-dimensional graphene aerogel as high-performance positive electrode materials for lithium-ion batteries. J Power Sources 340:40–50
13. Hao Y, Yan W, Jenq-Gong D (2018) Developing a novel diamine-assisted polymerization method to synthesize nano-$LiMnPO_4$ with N-doped carbon from polyamides for high-performance Li-ion batteries. Acs Sustainable Chemistry & Engineering: acssuschemeng.8b02868-
14. Xiong QQ, Lou JJ, Teng XJ, Lu XX (2018) Controllable synthesis of N-C@$LiFePO_4$ nanospheres as advanced cathode of lithium ion batteries. J Alloys Compd 743:377–382
15. Ding Y, Pan P, Chen L, Fu Z, Du J, Guo L, Wang F (2017) $LiFePO_4$ composites decorated with nitrogen-doped carbon as superior cathode materials for lithium-ion batteries. Ionics 23(12): 3295–3302
16. Xiong J, Wang Y, Wang Y, Zhang J (2016) PVP-assisted solvothermal synthesis of $LiMn_{0.8}Fe_{0.2}PO_4/C$ nanorods as cathode material for lithium ion batteries. Ceram Int 42(7):9018–9024
17. Li W, Zeng L, Wu Y, Yu Y (2016) Nanostructured electrode materials for lithium-ion and sodium-ion batteries via electrospinning. Sci China Mater 59(4):287–321
18. Li Q, Zheng F, Huang Y, Zhang X, Wu Q, Fu D, Zhang J, Yin J, Wang H (2015) Surfactants assisted synthesis of nano-$LiFePO_4/C$ composite as cathode materials for lithium-ion batteries. J Mater Chem 3(5):2025–2035
19. Bao L, Li L, Xu G, Wang J, Zhao R, Shen G, Han G, Zhou S (2016) Olivine $LiFePO_4$ nanocrystallites embedded in carbon-coating matrix for high power Li-ion batteries. Electrochim Acta 222:685–692
20. Arnold G, Garche J, Hemmer RP, Strobele S, Vogler C, Wohlfahrtmehrens M (2003) Fine-particle lithium iron phosphate $LiFePO_4$ synthesized by a new low-cost aqueous precipitation technique. J Power Sources 119:247–251
21. Cho T, Chung H (2004) Synthesis of olivine-type $LiFePO_4$ by emulsion-drying method. J Power Sources 133(2):272–276
22. Kim DH, Kim J (2006) Synthesis of $LiFePO_4$ nanoparticles in polyol medium and their electrochemical properties. Electrochem Solid-State Lett 9(9):A439–A442
23. Ding Y-H, Huang G-L, Li H-H, Xie H-M, Sun H-Z, Zhang J-P (2015) Double carbon nano coating of $LiFePO_4$ cathode material for high performance of lithium ion batteries. J Nanosci Nanotechnol 15(12):9630–9635
24. Li L, Fan C, Yang J (2018) A novel composite $Li_3V_2(PO_4)_3$‖$Li_2NaV_2(PO_4)_3/C$ as cathode material for Li-ion batteries. Aust J Chem 71(7):497–503
25. Yuan G, Ke C, Chen H, Hu X, Deng Z, Wei Z (2017) Surfactant assisted solvothermal synthesis of $LiFePO_4$ nanorods for lithium-ion batteries. J Energy Chem 026(3):564–568
26. Fan C, Li Q, Chen S, Fan J, Wen Z, Zeng T, Zhang X, Han S (2016) Poly (vinylpylrrolidone) as surfactant in the sol–gel preparation of

lithium iron phospate/carbon cathodes for lithium-ion batteries. Energy Technol 4(8):973–979
27. Chen S, Tang Q, Chen X, Tan L (2015) Nitrogen-doped carbon coated $LiFePO_4$/carbon nanotube interconnected nanocomposites for high performance lithium ion batteries. New J Chem 39(12): 9782–9788
28. (2015) Additives to disturb $LiMn_{0.8}Fe_{0.2}PO_4$growth and their influence on performance. J Nanopart Res 17(6):272
29. Zhao Z, Sun M, Chen W, Liu Y, Zhang L, Dongfang N, Ruan Y, Zhang J, Wang P, Dong L (2019) Sandwich, vertical-channeled thick electrodes with high rate and cycle performance. Adv Funct Mater 29(16):1809196
30. Novikova S, Yaroslavtsev S, Rusakov V, Chekannikov A, Kulova T, Skundin A, Yaroslavtsev A (2015) Behavior of $LiFe_{1-y}Mn_yPO_4$/C cathode materials upon electrochemical lithium intercalation/deintercalation. J Power Sources 300(30):444–452
31. Zhao N, Yongsheng LI, Zhi X, Wang L, Zhao X, Wang Y, Liang G (2016) Effect of $Ce^{3+}$ doping on the properties of $LiFePO_4$ cathode material. J Rare Earths 34(2):174–180
32. Yang X, Hu Z, Liang J (2015) Effects of sodium and vanadium co-doping on the structure and electrochemical performance of $LiFePO_4$/C cathode material for lithium-ion batteries. Ceram Int 41(2):2863–2868
33. Wang D, Li H, Shi S, Huang X, Chen L (2005) Improving the rate performance of $LiFePO_4$ by Fe-site doping. Electrochim Acta 50(14):2955–2958
34. Roberts MR, Vitins G, Owen JR (2008) High-throughput studies of $Li_{1-x}Mg_{x/2}FePO_4$ and $LiFe_{1-y}Mg_yPO_4$ and the effect of carbon coating. J Power Sources 179(2):754–762
35. Wang G, Bewlay S, Konstantinov K, Liu HK, Dou SX, Ahn J (2004) Physical and electrochemical properties of doped lithium iron phosphate electrodes. Electrochim Acta 50(2):443–447
36. Safronov DV, Novikova SA, Kulova TL, Skundin AM, Yaroslavtsev AB (2012) Lithium diffusion in materials based on $LiFePO_4$ doped with cobalt and magnesium. Inorg Mater 48(5): 513–519
37. Nakamura T, Sakumoto K, Okamoto M, Seki S, Kobayashi Y, Takeuchi T, Tabuchi M, Yamada Y (2007) Electrochemical study on $Mn^{2+}$-substitution in $LiFePO_4$ olivine compound. J Power Sources 174(2):435–441
38. Zaghib K, Mauger A, Goodenough JB, Julien CM (2012) Design and properties of $LiFePO_4$ nano-materials for high-power applications. Springer US, 8:179–220
39. Chung S, Bloking JT, Chiang Y (2002) Electronically conductive phospho-olivines as lithium storage electrodes. Nat Mater 1(2): 123–128
40. Moskon J, Pivko M, Jerman I, Tchernychova E, Logar NZ, Zorko M, Selih VS, Dominko R, Gaberscek M (2016) Cycling stability and degradation mechanism of $LiMnPO_4$ based electrodes. J Power Sources 303(30):97–108
41. Hu S, Pillai AS, Liang G, Pang WK, Wang H, Li Q, Guo Z (2019) Li-rich layered oxides and their practical challenges: recent progress and perspectives. Electrochemical Energy Reviews 1-35
42. Tianyu L, XiaoZi Y, Lei Z, Datong S, Kaiyuan S, Christina B (2020) Degradation mechanisms and mitigation strategies of nickel-rich NMC-based lithium-ion batteries. Electrochemical Energy Reviews 3:43–80
43. Sari HMK, Li X (2019) Controllable cathode–electrolyte interface of Li $[Ni_{0.8}Co_{0.1}Mn_{0.1}]O_2$ for lithium ion batteries: a review. Adv Energy Mater 9(39)
44. Liu W, Li X, Xiong D, Hao Y, Li J, Kou H, Yan B, Li D, Lu S, Koo A, Adair K, Sun X (2017) Significantly improving cycling performance of cathodes in lithium ion batteries: the effect of $Al_2O_3$ and $LiAlO_2$ coatings on $LiNi_{0.6}Co_{0.2}Mn_{0.2}O_2$. Nano Energy 44:111–120
45. Ruying L, Andrew L, Jian L, Mei C, Mohammad N (2014) Atomic layer deposition of solid-state electrolyte coated cathode materials with superior high-voltage cycling behavior for lithium ion battery application. Energy Environ Sci 2: 469–832
46. Kobayashi G, Yamada A, Nishimura SI, Kanno R, Kobayashi Y, Seki S, Ohno Y, Miyashiro H (2009) Shift of redox potential and kinetics in $Li_x$ $(Mn_yFe_{1-y})PO_4$. J Power Sources 189(1): 397–401
47. Liu W, Gao P, Mi Y, Chen J, Zhou H, Zhang X (2013) Fabrication of high tap density $LiFe_{0.6}Mn_{0.4}PO_4$/C microspheres by a double carbon coating–spray drying method for high rate lithium ion batteries. J Mater Chem A 1(7):2411–2417
48. Mi Y, Gao P, Liu W, Zhang W, Zhou H (2014) Carbon nanotube-loaded mesoporous $LiFe_{0.6}Mn_{0.4}PO_4$/C microspheres as high performance cathodes for lithium-ion batteries. J Power Sources 267: 459–468
49. Yang X, Mi Y, Zhang W, Wu B, Zhou H (2015) Enhanced electrochemical performance of $LiFe_{0.6}Mn_{0.4}PO_4$/C cathode material prepared by ferrocene-assisted calcination process. J Power Sources 275:823–830
50. Shen H, Xiang W, Shi X, Zhong B, Liu H (2016) Hierarchical $LiMn_{0.5}Fe_{0.5}PO_4$/C nanorods with excellent electrochemical performance synthesized by rheological phase method as cathode for lithium ion battery. Ionics 22(2):193–200
51. Xiang W, Wang E, Chen M, Shen H, Chou S, Chen H, Guo XD, Zhong BH, Wang X (2015) Hierarchical structured $LiMn_{0.5}Fe_{0.5}PO_4$ spheres synthesized by template-engaged reaction as cathodes for high power Li-ion batteries. Electrochim Acta 178: 353–360
52. Zhuo Z, Hu J, Duan Y, Yang W, Pan F (2016) Transition metal redox and Mn disproportional reaction in $LiMn_{0.5}Fe_{0.5}PO_4$ electrodes cycled with aqueous electrolyte. Appl Phys Lett 109(2): 023901
53. Zhou X, Xie Y, Deng Y, Qin X, Chen G (2015) The enhanced rate performance of $LiFe_{0.5}Mn_{0.5}PO_4$/C cathode material via synergistic strategies of surfactant-assisted solid state method and carbon coating. J Mater Chem 3(3):996–1004
54. Zhong Y, Li J, Wu Z, Guo X, Zhong B, Sun S (2013) $LiMn_{0.5}Fe_{0.5}PO_4$ solid solution materials synthesized by rheological phase reaction and their excellent electrochemical performances as cathode of lithium ion battery. J Power Sources 234:217–222
55. Deng Z, Wang Q, Peng D, Liu H, Chen Y (2019) Fast precipitation-induced $LiFe_{0.5}Mn_{0.5}PO_4$/C nanorods with a fine size and large exposure of the (010) faces for high-performance lithium-ion batteries. J Alloys Compd 794:178–185
56. Zhuang H, Bao Y, Nie Y, Qian Y, Deng Y, Chen G (2019) Synergistic effect of composite carbon source and simple precalcining process on significantly enhanced electro chemical performance of porous $LiFe_{0.5}Mn_{0.5}PO_4$/C agglomerations. Electrochim Acta 314:102–114
57. Huang YP, Tao T, Chen Z, Han W, Wu Y, Kuang C, Zhou S, Chen Y (2014) Excellent electrochemical performance of $LiFe_{0.4}Mn_{0.6}PO_4$ microspheres produced using a double carbon coating process. J Mater Chem 2(44):18831–18837
58. HuangKai Z, JinHua L, XiaoPeng H, YuanChao D, Feng L, YaoChun Y (2017) Improved electrochemical performance of $LiFe_{0.65}Mn_{0.35}PO_4$ cathode material by using electrolytic manganese dioxide for lithium-ion battery. SCIENCE CHINA Technol Sci 060(012):1853–1860
59. Zhi L, Xu Z, Tan X, Wang H, Holt CMB, Stephenson T, Olsen BC, Mitlin D (2013) Mesoporous nitrogen-rich carbons derived from protein for ultra-high capacity battery anodes and supercapacitors. Energy Environ Sci 6(3):871–878

60. Tao HC, Huang M, Fan LZ, Qu X (2013) Effect of nitrogen on the electrochemical performance of core–shell structured Si/C nanocomposites as anode materials for Li-ion batteries. Electrochim Acta 89:394–399
61. Dou L, Han E, Li L, Zhu L, Qiao S, Liu H (2018) Synthesis and electrochemical properties of Mg-doped and Al-doped $LiMnPO_4{\cdot}Li_3V_2(PO_4)_3$/C cathode materials for lithium-ion batteries. Ionics 25(6):2487–2499